Synthesis, physicochemical and vibrational spectral properties of 2–pyridone and 2–aminopyridine derivatives: An experimental and theoretical study

Synthesis, physicochemical and vibrational spectral properties of 2–pyridone and 2–aminopyridine derivatives: An experimental and theoretical study

Keshk R. M.; Garavelli M.; El-Tahawy M. M.

T.J. Mol. Structure **2021, 1225, 129136**

The final published version is available online at: https://dx.doi.org/10.1016/j.molstruc.2020.129136

Synthesis, Physicochemical and Vibrational Spectral Properties of 2–Pyridone and 2–Aminopyridine Derivatives: an Experimental and Theoretical Study

Reda M. Keshk[1*], Marco Garavelli[2*], Mohsen M. T. El–Tahawy[1,2*]

[1]Chemistry Department, Faculty of Science, Damanhour University, Damanhour 22511, Egypt

[2]Dipartimento di Chimica industriale "Toso Montanari", Università di Bologna, Viale del Risorigmento 4, 40136 Bologna, Italy.

*Corresponding authors

redakeshk@sci.dmu.edu.eg (R.K.)

marco.garavelli@unibo.it (M.G.)

mohsen.eltahawy@sci.dmu.edu.eg (M.E.)

ORCID

R.K.: 0000–0002–9782–4334

M.G.: 0000–0002–0796–289X

M.E.: 0000–0002–9561–9521

Abstract: A convenient and efficient one–pot three–component reaction of acetyl acetone, malononitrile and ammonium acetate was investigated for the synthesis of 3–cyano–4,6–dimethyl–2–pyridone (PI) and 2–amino–3–cyano–4,6–dimethylpyridine (PII). The products were achieved with high purity, high yields and short reaction time. The yields of the two products depend on the concentration of ammonium acetate, reaction time and the solvent used. The structures of the isolated products were confirmed by elemental analysis and spectral data, supported by quantum chemical (MP2) calculations, both in gas phase and solvents (water and ethanol), that were also employed to track the reaction mechanisms and model vibrational spectral properties for final characterization and interpretation of spectral data. A remarkable matching between theoretical predictions and experiments was attained both for the geometrical parameters, as compared to X-Ray data available in the litterature, and for vibrational frequencies, leading to a correlation coefficient (R^2) of 0.99.

Keywords

Cyanopyridine; MP2; Solvent Effect; Vibrational Scale Factor; Reaction Mechanism; Energy Profile; Molecular Properties

Introduction

Pyridine derivatives are well known for their versatile biological activities such as anticancer [1], antimicrobial [2, 3], antiviral [4], anticonvulsant [5] and anti–human immunodeficiency viruses (AntiHIV)[6]. Cyanopyridines (nicotinonitriles) are associated with diverse pharmacological and chemotherapeutic activities as antitumor [7], protein kinase inhibitors [8], anxietic [9], antimicrobial [10] and antitubercular[11]. They have been also used as intermediates for the synthesis of vitamins and as ligands for transition metal ions in the formation of the nuclear factor kappa–β kinase subunit beta inhibitor (IKK–β–inhibitor) drug complexes[11]. 2–pyridones are biologically interesting molecules as they act as inhibitors of phosphodiesterase 3 (PDE3) a target for heart failure and platelet aggregation[12], anticancer agents[13], antiviral, antimicrobial, antiepilepsy, antidiabetic[14] and their chemistry has received considerable attention [15-20]. Thus, despite the large number of methods known for their synthesis, new procedures are continuously being developed [21, 22]. The Guareschi pyridone (3–cyano–4,6–dimethyl–2–pyridone) is

one of the most important methods for the synthesis of 2–pyridone from 1,3–diketone (PI) [23]. Catalysts such as zeolite [24], piprazine, piprazine carboxy aldehyde, and triethylamine [25] have implied in the synthesis of this compound. Specifically, F. A. Yassin has prepared PI and its derivatives through the reaction of cyanoacetamide and acetylacetone using piperidine as a catalyst in boiling n–butanol solvent[26].

Considerable attention to the synthesis of 2–amino–3–cyanopyridine derivatives is drawn by their interesting biological activity and photophysical properties. These compounds may act as ligands of adenosine receptors [27-29], inhibitors of activated protein kinase–2 for treatment of diseases caused by the tumor necrosis factor (TNFα) [30], as well as inhibitors of human cytomegalovirus [30], anti–inflammatory agents [31] and possess anti–microbial activity [32-36]. They were employed as an efficient organic catalyst in the facile synthesis of pharmaceutically important compounds[37, 38], on the other hand they work as inhibitor for corrosion of mild steel in acidic medium[39]. Additionally, they are promising in the development of agents for treatment of cardiovascular conditions [28]. Various approaches to the synthesis of these derivatives have been reported, including microwave irradiation[40], ultrasound irradiation [41, 42], reaction with hexadecyldimethyl benzyl ammonium bromide and triethylamine[43], and dimethylformamide (DMF)[44]. However, most of these methods suffer from several drawbacks like harsh reaction conditions, prolonged reaction times and low yields.

In view of these facts, the development of new methods for the synthesis of cyanopyridine derivatives is pursued. In this work, a new strategy for the synthesis of 3–cyano–4,6–dimethyl–2–pyridone and 2–amino–3–cyano–4,6–dimethylpyridine is introduced, involving combination of acetyl acetone, malononitrile and ammonium acetate. To the best of our knowledge, neither quantum chemical calculation, nor vibrational spectra analysis of the title molecules have been reported. Consequently, the experimental work is accompanied by a quantum chemical study to investigate the structural parameters, reaction pathways and vibrational spectroscopic properties of the synthesized compounds, together with the study of the solvent effect on the molecular properties.

Experimental Details

All the chemicals used in the synthesis were purchased from Fluka and Sigma. Melting points were measured by MEL_TEMP II apparatus and are uncorrected. IR spectra (KBr) were recorded on Perkin–Elmer FT/IR spectrophotometer scanning between 400 and 4000 cm^{-1}, ^{1}H NMR and ^{13}C NMR spectra were obtained on JEOL (500 MHz) in DMSO–d_6 as solvent. Chemical shifts values are expressed in ppm relative to tetramethyl–silane (TMS) as internal reference standard. The IR and NMR spectra were performed at Faculty of Science, Alexandria University. Elemental analysis (C, H, and N) was performed by a Vario III CHN analyzer (Germany) at the Microanalytical Unit of Cairo University. Compounds were within ± 0.4% of the theoretical values. Mass spectra were run on DI analysis Shimadzu QP–2010 plus mass spectrometer at the Microanalytical Unit of Cairo University. The purity of the compounds and the progress of the reaction were monitored by TLC analytical silica gel plates 60 F_{254} using (ethyl acetate, and n–hexane) and UV lamp was applied for spot visualization.

Synthesis of 3–cyano–4,6–dimethyl–2–pyridone (PI) and 2–amino–3–cyano–4,6–dimethylpyridine (PII)

Method A:

Malononitrile (0.1 mol) and ammonium acetate (0.05 mol or 0.1 mol or 0.2 mol) were added to a solution of acetyl acetone (0.1 mol) in ethanol absolute (200 mL). The reaction was refluxed in water bath for the appropriate time as reported in **Table 1**. The formed precipitate was filtered on hot and washed several times with hot ethanol followed by washing with excess water and dried to afford **PI** (crystallized from mixture of DMF/ethanol (1:1) or acetic acid). The filtrate was concentrated, poured into crushed ice after cooling. The formed precipitate was filtered off, washedby water then dried to afford **PII** (crystallized from ethanol).

Method B:

To solution of acetyl acetone (0.1 mol) were added in glacial acetic acid (200 mL), malononitrile (0.1 mol) and ammonium acetate (0.05 mol or 0.1 mol or 0.2 mol). The reaction was refluxed for the appropriate time as reported in **Table 1**. The reaction mixture was left to cool at room temperature, the formed precipitate was filtered off

and washed several times with acetic acid followed by washing with excess water then dried to afford **PI** (crystallized from acetic acid or DMF/ethanol mixture). The filtrate was concentrated, poured into crushed ice after cooling then neutralized with ammonium hydroxide. The formed precipitate was filtered off, washed by water then dried to afford **PII** (crystallized from ethanol).

Computational details

The geometry optimizations of the investigated reactants, intermediates and products either in gas phase or in solvents (ethanol and acetic acid) were carried out using ab initio Moller–Plesset second–order perturbation MP2 method [45] which better estimates the correlation energy and the vibrational spectra for the class of studied molecules[46-48]. Geometry optimizations were performed without any constrain implying a relatively large–size basis set 6–311++g(d,p) [49, 50] where two diffuse and two polarized functionals were included to better account for the electron density. Frequency calculations were performed on top of the optimized structures at the same level of theory to ascertain their nature (minima or transition states).
The solvent effect on the molecular properties were investigated by the integral equation formalism polarized continuum model (IEFPCM) [51]. This model is a modified version of PCM in which the cavity is considered as overlapping atomic spheres that are 20% larger than the van der Waals radii [52, 53]. All calculations have been carried out using Gaussian 09 [54], while GaussView 6 is used to visualize and assign the mode of vibrations.

Results and discussion

The reaction of acetyl acetone with malononitrile in the presence of ammonium acetate afforded a mixture of 3–cyano–4,6–dimethyl–2–pyridone (**PI)** and 2–amino–3–cyano–4,6–dimethylpyridine (**PII)** (**Scheme 1**). The reaction was carried out using different solvents, different concentrations of ammonium acetate and different reaction times to achieve a suitable condition for the synthesis of the two products. **Table 1** reports the yields of the two products at different reaction conditions. The obtained data showed high yield of 3–cyano–4,6–dimethyl–2–pyridone (**PI)** formation compared with 2–amino–3–cyano–4,6–dimethylpyridine (**PII)** in both solvents in short reaction times. This may be due to ammonium acetate

catalyzed the formation of **PI** at short reaction time. To study the solvent effect, ethanol (for environmental acceptability and cheapness) and acetic acid (for easier separation of the products from reaction mixture) were used.

PII has higher yield in ethanol solvent, as compared to acetic acid. This may be attributed to the higher dissociation affinity of the ammonium acetate (a source of ammonia)in ethanol than in acetic acid (Lechatelier's principle). Also, the data showed remarkable decrease in **PI** yield in ethanol compared to acetic acid. So, the best solvent for **PII** synthesis is ethanol while acetic acid for **PI** synthesis. Furthermore, theobtained date showed gradual increase in **PI** and **PII** yields with increasing ammoniumacetate concentration (from 0.05mol to 0.1mol). Which showed the role of ammonium acetate in the reaction (catalyzed **PI** synthesis and ammonia source for **PII**synthesis). Further increase in ammonium acetate concentration directed the reaction to **PII** synthesis. On the other hand, as expected, the reaction time showed great effect on the yield percent of the two products: where increasing the reaction time enhanced the yield of the products at low concentration of ammonium acetate (0.05 mol). Moreover, extending the reaction time (at the low or high ammonium acetate concentration) directed the reaction to the **PII** synthesis with gradual decrease in the **PI** percentage. This supported the reaction of **PI** with ammonium acetate to give **PII**. High concentration of ammonium acetate and longer reaction time afforded compound **PII** in good yields due to reaction of the formed **PI** with ammonia.

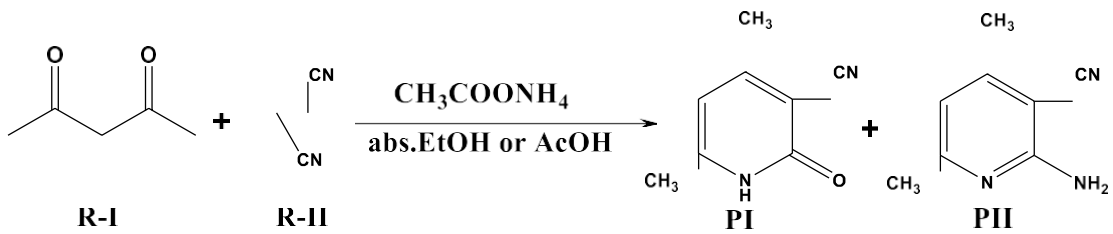

Scheme 1

The formation of compound **PI** is expected to proceed by condensation between acetyl acetone and malononitrile to afford compound **MI–II** which converted to its enol form **MI–2**; the latter cyclizes to **MI–3** followed by rearrangement to afford **PI** (**Scheme 2**), while the formation of **PII** is expected to proceed by reaction of compound **MI–II** with ammonia to yield **MII–2** which then cyclizes to **PII** (**Scheme 3**)

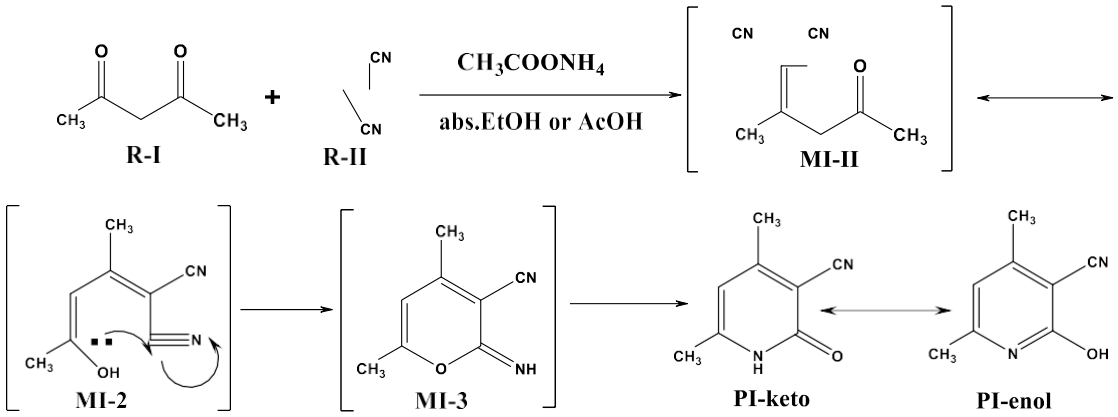

Scheme 2

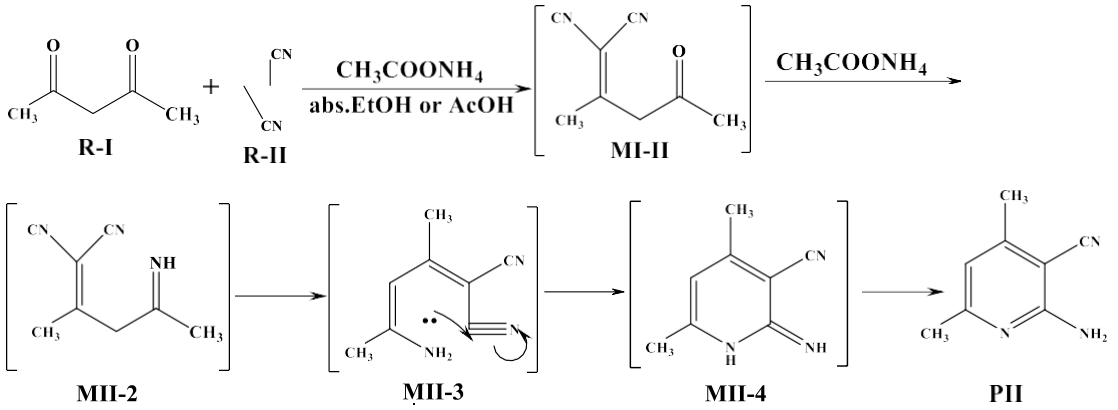

Scheme 3

Table 1 Optimization of solvent, ammonium acetate conc. and reaction time in the synthesis of PI and PII

Solvent	[CH_3COONH_4]	Reaction time (min)	PI yield %	PII yield %
AcOH	(0.05mol) (3.85g)	30	73%	10%
		60	76%	12%
		120	73%	14%
	(0.1mol) (7.7g)	30	78%	12%
		60	74%	15%
		120	70%	17%
	(0.2mol) (15.4g)	30	72%	19%
		60	69%	22%
		120	67%	25%
EtOH	(0.05mol) (3.85g)	30	72%	11%
		60	73%	13%
		120	70%	17%
	(0.1mol) (7.7g)	30	75%	14%
		60	71%	18%
		120	68%	21%

	30	70%	22%
	60	66%	26%
(0.2mol) (15.4g)	120	64%	29%
	5*60	44%	47%
	10*60	16%	76%

Reaction Mechanisms

In the gas phase, according to our calculations, the reactant I (R–I) adapts symmetrical geometrical parameters where both the two C=O bonds display equal bond length (1.22 Å); also the two C–C bonds between the carbonyl groups are identical in bond length (1.53 Å) while the other C–C bonds are slightly shorter (1.51 Å). In the same way the charge is distributed in symmetric way over the entire molecule where the oxygen atoms bear negative charge of–0.64e each while each adjacent carbon atom has a positive charge of +0.67e. Each oxygen atoms makes a dihedral angle equals 90º with the three centered carbon atoms, the bond angle of these atoms is slightly deviated from the tetrahedral value to be 104º. Calculations in solvents (ethanol and acetic acid) show limited changes either in bond lengths or in bond angles, the only noticeably changes related to the charge distribution where the negative charge on the oxygen atoms is slightly enhanced to–0.68e and–0.69e in acetic acid and ethanol, respectively; the same is true for the positive charge on the carbonyl carbon which is changed to +0.71e and +0.72e in acetic acid and ethanol, respectively (see SI).

The same situation is also shown for reactant II, where in gas phase it displays a completely symmetric structure with the two CN bonds lying in the same plane; this planarity is slight broken down by about 2º in both solvents. Moreover, the charge distribution is also modified in solution where negative charge on nitrogen atoms is changed from–0.32e to–0.38 on going from gas phase to solvent calculations. On the other hand, the CN and CC bond display lengths of 1.173 Å and 1.468 Å respectively (according to their triple and single bond character) and are not affected upon solvation.

The proposed reaction mechanisms can be directly accounted for in terms of potential energy changes going from reactants, to intermediates and eventually to the final products, see Fig. 1. The reaction of I and II occur though the intermediate MI–II. This step is an endothermic process by ca. 3.9, 5.0 and 4.6 kcal/mol in gas phase,

ethanol and acetic acid respectively, Fig. 1 (left panel). Ongoing from gas phase to the solvents, the MI–II shows a stabilization of 12.8 and 10.3 kcal/mol in ethanol and acetic acid, respectively. The charge distribution on MI–II is completely different than on the reactant compounds. The formation of MI–II is followed by 1,3 hydrogen shift which required additional energy of about 12 kcal/mol to afford the intermediate MI–2. The hydrogen shift preserves of intermediates relative stability where both MI–II and MI–2 intermediates are more stable in ethanol than in acetic acid by ca. 2.5 kcal/mol in. On the other hand, a change in the planarity of the molecule is observed where the C–O moiety is aligned in the same plane of the neighboring carbon atoms in MI–2 instead of being perpendicular as in MI–II intermediate. Such alignment allows spontaneous ring closure leading to an exothermic process for MI–3 intermediate formation (ca.–13.5,–12.1 and–12.2 kcal/mol in gas phase, ethanol and acetic acid, respectively), see Fig. 1 (left panel). Eventually, MI–3 affords the final product PI in the final step, which is extremally exothermic (ca.–28,–32 and–31 kcal/mol for gas phase, ethanol and acetic acid, respectively). This product exhibits two toutomeric forms, i.e. Lactam (PI-keto) and Lactim (PI-enol). Calculations show that PI-enol is more stable in gas phase by only ca. 1 kcal/mol in agreement with the experimental results of Break [46], while PI-keto is more stable in solvents by ca. 5.9 and 4.6 kcal/mol in ethanol and acetic acid, respectively, due to its tendency to form hydrogen bonds with the solvents [47]. On the other hand, the PI-keto in both solvents nearly shows the same stability, which accounts for the comparable yields observed in both cases. In all cases, the overall reaction is exothermic by ca.–25.6 kcal/mol in gas phase and–26.6 kcal/mol in both solvents. Moreover, the reaction is accomplished through a barrier which increase in the order gas (15.9 kcal/mol) < acetic acid (16.4 kcal/mol) < ethanol (16.9 kcal/mol). This order could explain the relative higher yield observed in acetic acid as compared to that in ethanol (e.g. 73% vs. 70% for acetic acid and ethanol, respectively).

The first step toward the formation of the product II (PII) is similar as in case of PI, i.e. the formation of MI–II. The next step is an endothermic reaction of ca. 6 kcal/mol between the ammonia and this intermediate, giving the intermediate MII–2 (see Fig. 1, right panel). The later displays a stability, with respect to the gas phase, of ca. 13 and 10 kcal/mol in ethanol and acetic acid, respectively. This step is followed by almost a barrierless 1,3 hydrogen shift from the carbon to the nitrogen to form the

intermediate MII–3, which displays a nearly planar geometry. Repeatedly, as in case of PI formation, MII–3 performs a ring closure to form the MII–4 in an exothermic step of ca.–24.4,–23.3 and–23.5 in gas phase, ethanol and acetic acid, respectively. In a further exothermic step, a 1,3–hydrogen shift in MII–4 affords the final product PII. The overall reaction of PII formation is exothermic by–29.6,–25.7 and–24.4 kcal/mol in gas phase, acetic acid and ethanol, respectively, with a barrier order of gas (12.0 kcal/mol) < acetic acid = ethanol (11.6 kcal/mol), see Fig. 1(right panel).

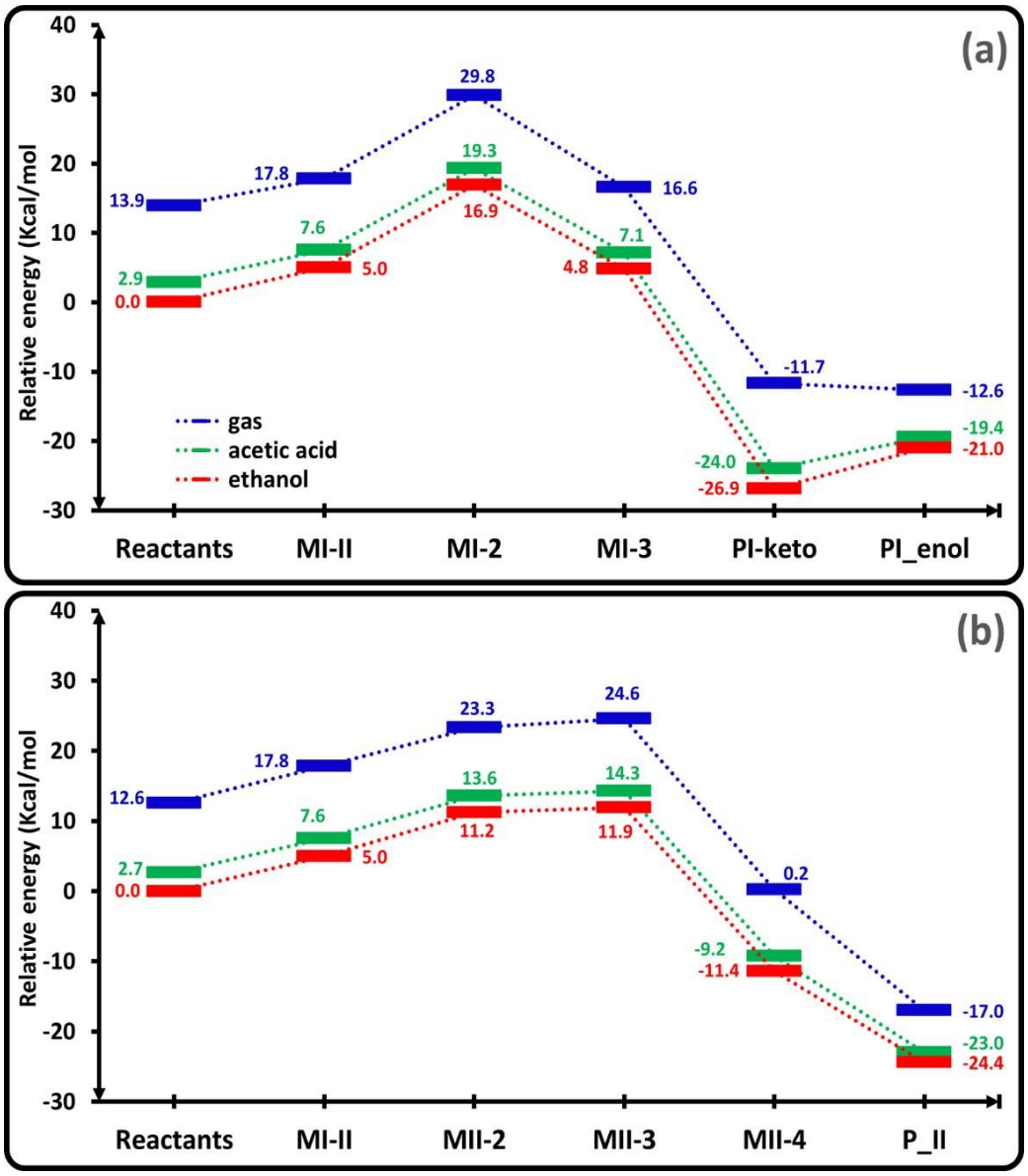

Fig. 1 The potential energy profile for the reaction path of PI (a) and PII (b), in gas phase, ethanol and acetic acid.

Geometrical parameters of the products PI and PII

Generally, solvent has very tinny effect on the calculated geometrical parameters i.e. bond lengths, bond angles, and dihedral angles, therefore hereafter we will discuss the result calculated in gas phase in comparison to available single–crystal X–ray data. Data computed in solvents are reported in the supporting information (see below). The optimized geometries for the PI–keto and PII are shown in the Fig. 2. Consistently with its experimental rotational parameter [57, 58], the ground state geometry of PI–keto is slightly distorted from planarity by ca. 5° as confirmed form the dihedral angle value within the pyridine ring (i.e. N_1–C_2–C_3–C_4, C_2–C_3–C_4–C_5, C_3–C_4–C_5–C_6, C_4–C_5–C_6–N_1, C_5–C_6–N_1–C_2 and C_6–N_1–C_2–C_3), their computed values are agree with the crystallographic values for the unsubstituted compound[59], Table 2. In contrast, the crystal X–ray structure of PI [23] displays almost planar geometry with only a deviation of ca. 1.1° for the D values of N_1–C_2–C_3–C_5 and C_2–C_3–C_4–C_5. Their corresponding computed values are 5.5 and 4.3°, respectively. Such small deviation could be attributed to the different phase (solid vs. vacuum). This conclusion was further supported by the enhanced observed planarity in solvent calculations (corresponding data calculated in solvents are reported in the supporting information, Table S1). The carbonyl and cyano groups are in the same plane as established from the calculated and experimental D values of both O_7–C_2–C_3–C_8 and O_7–C_2–C_3–N_9, see Table 2. All the other dihedral angles show considerable matching between the estimated and experimental values, see Table 2. In the same way, all the calculated bond distances of C_1–C_2, C_2–O_7, C_3–C_4, C_4–C_5, C_5–C_6 and C_3–C_8 are 1.403, 1.225, 1.383, 1.425, 1.372 and 1.431Å respectively, within ~0.01 Å the corresponding experimental ones, whereas the calculated values of N_1–C_6 and C_2–C_3 are 1.463 and 1.367 Å i.e. slightly off the experimental one by ca. –0.02 and –0.03Å, respectively. The nitrile group which displays the standard linear structure has a bond distance of 1.130 Å deviated by ca. –0.05 Å from the calculated value. On the other hand, all the calculated and the experimental bond angle are in well agreement (within only ±3°). The good agreement between experimental and calculated geometrical parameters demonstrate the reliability of the computational model employed to study such organic systems.

To the best of our knowledge, there is no available cyclographic data available for PII, therefore we will discuss its calculated parameters in comparison with

experimental values of the 2–amino pyridine. Generally, PII displays a geometry very close to that of PI, see Table 2. The bond lengths of C_3–C_8, C_8–C_9, C_4–C_{10} and C_6–C_{11} show almost the same value calculated for PI, some other bonds such as C_3–C_4, C_4–C_5, C_5–C_6 and C_6–N_1 are deviated by ca. ±0.02Å form the calculated values of PI. On the other hand, the N–C_2 and C_3–C_4 bonds are increased by ca. 0.06 and 0.05Å compared to their PI values, this effect being mainly attributed to the conjugation of the amino group with the pyridine ring. This conjugation is confirmed from the calculated bond distance (1.381Å) of the C_2–N_7 bond which shows double bond character (a typical value for a single C–N bond is 1.43 Å [60]). Moreover, all the calculated bond distances are in a good agreement with the experimental values reported for the unsubstituted 2–amino pyridine [61] within a slight deviation of ca. ±0.02Å.

The exchange of the O and NH_2 groups in the pyridine ring at position 2 in PI and PII shows an observed effect on the calculated bond angles of the neighboring moiety where in PII the N_1–C_2–C_6 bond angle is increased by ca. 10° while C_2–C_1–C_6 is decreased by 8° compared to their values in PI. The other bond angles are slightly modified by this substitution. In all cases, all the calculated bond angles matches perfectly their experimental values [61]. Moreover, as in the case of PI, PII is slightly distorted form planarity by ca. 4° which is in agreement with the experimental assignment [61]; however this is not the case for unsubstituted pyridine which displays completely planar ring [62]. The substitution of O and NH_2 groups also affects the calculated NBO charge density where all atomic charges are slightly modified by ca. ±0.03e except for the atom at substitution position that is changed from –0.77e to –0.55 for PI and PII, respectively.

The chemical reactivity of the reacting species mainly depends on the interaction among the frontier molecular orbitals (FMO), i.e. the highest occupied molecular orbital (HOMO) and the lowest unoccupied molecular orbital (LUMO)[63, 64]. The HOMO is associated with the ability of the molecules to donate electrons while the LUMO provides a measure for the molecules' affinity to accept electrons. The HOMO and the LUMO are depicted in Fig. 2 for calculations in gas phase, whereas HOMO and LUMO for calculations in solvents, as well as the contribution of the atoms and atomic orbitals in their composition, are shown in the supporting information (Figure S7, Figure S8 and Table S2, Table S3, respectively). Calculation in gas phase on PI shows that the HOMO is mainly localized over C_5(54%) with small contribution from

C_3(9%), C_4(14%) and C_5(8%) atoms; in solvents other atoms participate in the composition of HOMO such as O_7(9%) and N_1(7%). The LUMO in vacuum is delocalized over C_8(24%), N_9(19%), C_3(20%), C_4(10%), C_5(11%), C_2(8%) and C_6(5%) while in solvents, only C_1, C_5, C_{15} and N_{18} atoms contribute by ca. 27%, 42%, 14% and 13%. On the other hand, in PII, the solvent has no significant effect on the shape of the HOMO and LUMO, where the HOMO is being delocalized over the ring and C_8, N_9 and N_7 while the LUMO is mainly localized over the C_8N_9(66%) group.

Dipole moments for PI and PII were also calculated at the same level of theory. The dipole moment is a function of the molecular charge distribution and can be considered as an indicator for the direction of charge transfer between positive and negative centers of the investigated molecule. The calculated value of dipole moment for PI is 8.4 D, which is in a good agreement with the experimental value of 8.8 D for the isolated molecule [56]. This value is slightly enhanced in acetic acid and ethanol to 10.9 and 11.5 D, respectively, while PII possess small dipole moment values of 3.2, 4.0 and 4.2D in gas, acetic acid and ethanol, respectively.

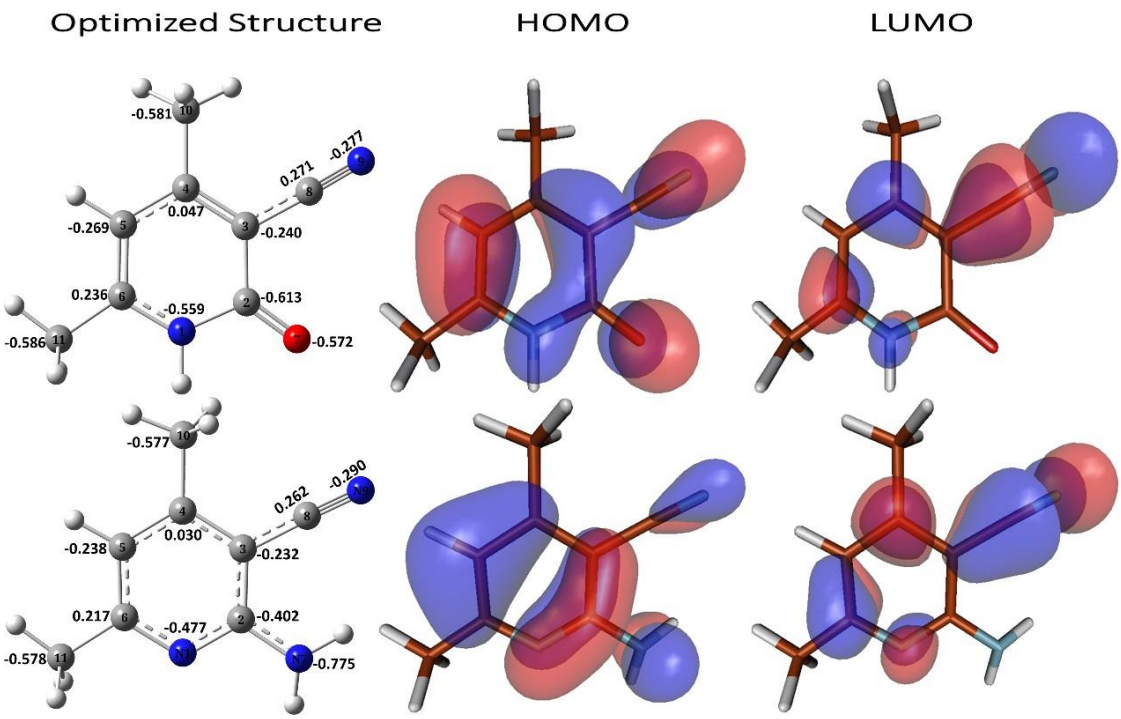

Fig. 2 The optimized geometry, HOMO and LUMO of PI (top) and PII (bottom) in vacuum; NBO charge distribution of the non–hydrogen atoms as well as the atom numeration employed in this work are reported on the optimized structures (the corresponding figures for calculation in ethanol and acetic acid are reported in the supporting information).

Table 2 Experimental and computed geometrical parameters of PI and PII in their vacuum ground electronic state (corresponding calculations in solvents are reported in the supporting information, Table S1).

	PI		PII	
Parameter	**Exp.[A]**	**Calc.**	**Exp.[B]**	**calc.**
N_1–C_2	1.389	1.403	1.336	1.339
C_2–$O_7(N_7)$	1.235	1.225	1.384	1.381
C_2–C_3	1.432	1.463	1.399	1.416
C_3–C_4	1.388	1.383	1.391	1.402
C_4–C_5	1.411	1.425	1.376	1.397
C_5–C_6	1.357	1.372	1.372	1.400
C_6–N_1	1.350	1.367	1.332	1.345
C_3–C_8	1.446	1.431	–	1.430
C_8–N_9	1.130	1.178	–	1.179
C_4–C_{10}	1.502	1.506	–	1.505
C_6–C_{11}	1.504	1.500	–	1.505
N_1–H	0.929	1.016	–	–
C_5–H	0.930	1.085	–	1.086
N_1–C_2–C_3	113.6	112.5	123.9	122.2
C_2–C_3–C_4	122.8	122.4	116.7	119.6
C_3–C_4–C_5	118.5	119.1	119.5	117.0
C_4–C_5–C_6	119.6	120.4	119.3	120.0
C_5–C_6–C_1	120.5	118.6	123.1	122.5
C_2–N_1–C_6	125.0	126.6	117.5	118.6
C_2–N_1–H13	117.5	113.6	–	53.2
C_6–N_1–H13	117.4	119.5	–	66.4
N_1–C_2– $O_7(N_7)$	120.6	120.9	117.2	116.7
C_3–C_2–$O_7(N_7)$	125.8	126.5	121.7	121.0
C_2–C_3–C_8	116.6	116.7	119.2	119.3
C_4–C_3–C_8	120.6	120.7	–	121.0
C_3–C_4–C_{10}	121.2	121.5	118.2	120.7
C_5–C_4–C_{10}	120.3	119.3	–	122.3
C_4–C_5–H	120.2	120.2	119.2	120.0
C_6–C_5–H	120.2	119.4	–	120.0
C_5–C_6–C_{11}	123.9	124.7	123.2	121.6
N_1–C_6–C_{11}	115.6	116.6	–	115.9
C_3–C_8–N_9	178.7	178.1	–	178.2
$O_7(N_7)$–C_2–C_3–C_4	178.6	176.0	–	177.6
$O_7(N_7)$–C_2–N_1–C_6	178.7	175.8	–	176.4
N_1–C_2–C_3–C_4	1.1	5.5	–	2.7
C_2–C_3–C_4–C_5	1.1	4.3	–	3.0
C_3–C_4–C_5–C_6	1.0	2.5	–	2.1
C_4–C_5–C_6–N_1	0.8	2.4	–	0.8
C_5–C_6–N_1–C_2	0.9	4.3	–	0.3
C_6–N_1–C_2–C_3	1.0	5.5	–	1.3
H–N_1–C_2–$O_7(N_7)$	1.6	1.9	–	163.7
H–N_1–C_2–$O_7(N_7)$	1.6	1.9	–	163.7
N_1–C_2–C_3–C_8	179.3	178.9	–	178.3
C_2–C_3–C_8–C_9	148.5	165.8	–	0.7
C_4–C_3–C_8–C_9	29.8	18.4	–	174.9
C_2–C_3–C_4–C_{10}	179.3	179.1	–	178.6
C_4–C_5–C_6–C_{11}	179.6	179.5	–	179.4
$O_7(N_7)$–C_2–C_3–C_8	0.4	0.3	–	6.8
$O_7(N_7)$–C_2–C_3–N_9	0.8	0.1	–	6.8

A and B: values taken from references[23] and [61] for PI and 2–amino pyridine, respectively.

Calculated and experimental vibrational modes in PI and PII

The optimized structural of the investigated molecules were used to compute the vibrational frequencies at MP2 level of theory. The linear correlation between the experimental frequencies and the corresponding unscaled harmonic calculated for PI and PII compounds are graphically depicted in Fig. 3, top panels while the experimental and theoretical IR spectra are shown in Figs. 3, bottom panels. Generally, there is a certain agreement between the unscaled and experimental frequencies, however, in some cases, considerable deviations exist. To overcome these disagreements, two different methods were used to scale the calculated wavenumbers: in the first method (M1), a uniform scaling factors of 0.98 and 0.94 are used for wavenumbers smaller and larger than 1,700 cm^{-1}, respectively [65-67], while in the second method (M2), the scaling procedure is generated from the linear relationship equations calculated from the graphs, (see Fig. 3, top panel), leading to $v_{scaled} = 0.94v_{unscaled} + 48.7$ and to $v_{scaled} = 0.91v_{unscaled} + 60.0$ for PI and PII, respectively (where v_{scaled} and $v_{unscaled}$ are the scaled and unscaled frequencies, respectively). Corresponding graphs for the calculation in ethanol and acetic acid are reported in the supporting information, Figs S8 and S13. Generally, the solvent effect does not show considerable effect neither on the calculated frequencies nor their intensities, see Table SXX in supporting information. The scaled frequencies, force constants (FC), relative IR intensities (Rel. Int.) and Raman activities of the vibrational modes of PI and PII in comparison to their experimental values are reported in Tables 3 and 4. Theoretically, PI and PII compounds possess 51 and 54 normal modes of vibrations, respectively. The illustration of these normal vibrational modes are shown in the supporting information Figs. SXX4. Very remarkably, a correlation coefficient (R^2) of 0.99 was obtained for M2 (see top panels of Fig. 3).

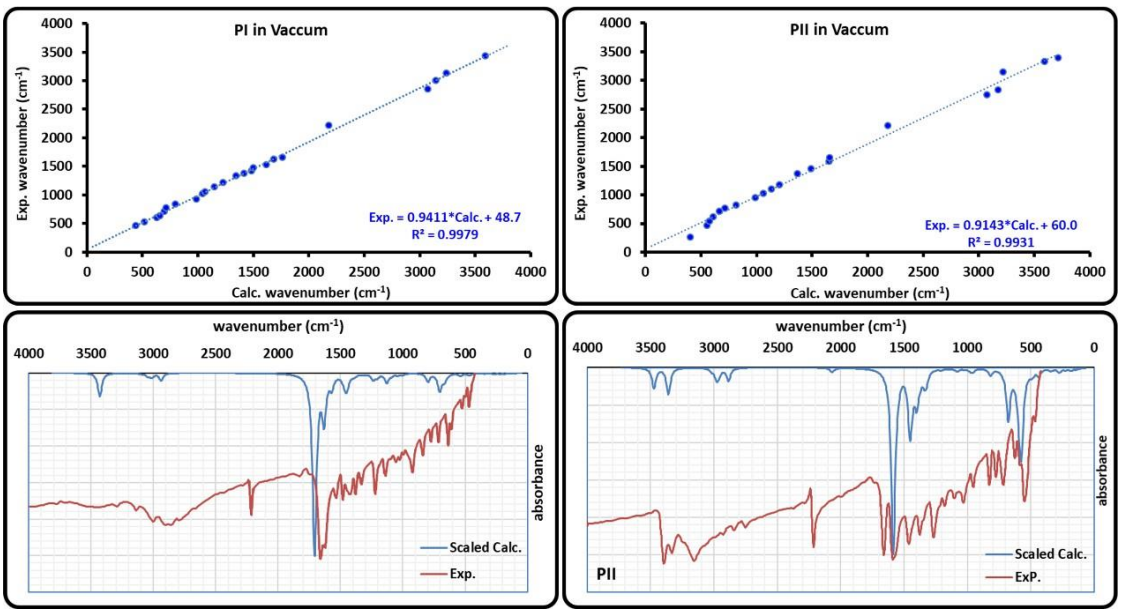

Fig. 3 Top: (Top) Linear correlation between of the experimental and unscaled calculated wave numbers; (Bottom) the experimental and scaled calculated (Method M2) vibrational spectra of PI and PII in vacuum.

Table 3 Experimental and calculated vibrational Frequencies of PI in vacuum.

mode	frequency Exp.	unscaled	scaled M1	scaled M2	FC	Relative IR intensity exp.	calc.	Raman activity	Assignment
1	–	51	50	96	0.0	–	0.1	0.3	Rot CH_3
2	–	75	74	119	0.0	–	0.0	0.3	Rot CH_3, Rot CN
3	–	117	114	158	0.0	–	0.1	0.2	Rot CH_3
4	–	140	137	181	0.1	–	0.1	3.0	ɣC–H, Rot CN
5	–	142	139	182	0.1	–	0.3	0.5	ɣ CH_3, ɣC≡N
6	–	182	178	220	0.1	–	0.3	0.8	p–CC, p–NH, ɣC–H
7	–	233	229	268	0.2	–	0.6	0.4	ɣ–C≡C, ɣ– CH_3
8	–	279	273	311	0.1	–	0.0	0.3	p–CC
9	–	316	310	346	0.3	–	0.3	1.4	ɣ–CC, ɣ– CH_3
10	–	415	407	439	0.6	–	0.2	1.8	p–ring
11	464	442	433	465	0.7	50.7	0.7	6.8	τ–C–C, τ–ring
12	–	448	439	471	0.9	–	0.4	1.4	p–C–C, P– CH_3
13	–	508	498	527	0.7	–	0.4	3.1	τ–ring
14	524	519	509	537	0.6	51.1	0.8	1.3	τ–ring, ɣ–N–H
15	–	527	517	545	1.0	–	0.3	10.4	τ–ring
16	–	605	593	618	1.1	–	0.1	2.0	ɣN–H, ɣC–C
17	610	629	616	641	1.2	57.8	0.6	0.6	R–C–C
18	637	656	643	666	0.5	63.3	3.7	21.5	ɣN–H
19	714	695	681	703	0.9	62.0	9.1	6.8	ring–breathing
20	772	711	697	718	1.6	61.7	0.6	4.1	δ–ring, δ–CH3
21	840	796	780	798	0.4	66.2	4.4	7.1	ɣC–H
22	924	985	965	975	1.1	72.0	0.0	0.8	R– CH_3
23	–	1009	988	998	2.2	–	0.7	4.3	δ–ring, R– CH_3
24	1025	1045	1024	1032	1.0	67.8	0.3	6.6	R– CH_3
25	–	1053	1032	1039	1.0	–	0.5	0.2	p– CH_3
26	1053	1065	1044	1051	1.0	68.5	0.3	2.5	τ– CH_3
27	–	1108	1086	1092	1.9	–	1.0	0.0	τ– CH_3, R–NH
28	1139	1148	1125	1129	3.5	72.9	5.0	1.2	δ–ring, δ–CH
29	1221	1228	1204	1205	1.4	78.9	2.0	1.4	δ– CH
30	–	1263	1238	1238	3.6	–	3.2	31.1	δ–NH
31	1332	1341	1314	1311	2.6	75.8	0.3	10.8	δ–CH, δ–NH
32	1378	1419	1390	1384	1.5	79.0	0.8	16.2	δ– CH_3
33	–	1427	1398	1391	1.5	–	0.3	22.9	δ– CH_3
34	–	1445	1416	1409	3.2	–	0.5	6.2	δ–NH, δ– CH_3
35	1426	1485	1455	1446	2.1	78.9	5.1	29.8	v–C–N, δ–NH, δ– CH_3
36	–	1493	1463	1454	1.4	–	1.5	17.1	τ CH_3
37	1480	1499	1469	1460	1.5	80.8	2.8	8.6	τ CH_3, δ–NH
38	–	1508	1478	1468	1.5	–	2.0	8.9	τ CH_3
39	–	1528	1498	1487	2.2	–	0.8	12.6	δ–CH_3, δ–NH, δ–CH
40	1536	1616	1584	1569	10.3	80.2	6.6	14.9	v–C=C
41	1625	1682	1648	1631	9.4	96.3	24.6	6.0	v–C=C
42	1659	1762	1656	1707	16.1	100.0	100.0	10.9	v–C=O
43	2217	2182	2052	2103	35.4	85.6	0.2	58.4	v–C≡N
44	2854	3071	2886	2939	5.8	88.7	2.9	19.0	v–CH3(s.)
45	–	3071	2887	2939	5.8	–	1.2	400.2	v–CH3 (as.)
46	3003	3146	2957	3010	6.4	87.8	0.9	178.9	v–CH3 (as.)
47	–	3152	2962	3015	6.4	–	1.4	263.0	v–CH3 (as.)
48	–	3180	2989	3041	6.6	–	0.8	56.1	v–CH3 (as.)
49	–	3187	2996	3048	6.6	–	0.9	84.6	v–CH3 (as.)
50	3138	3240	3046	3098	6.8	84.1	0.4	48.6	v–CH (aromatic)
51	3434	3593	3377	3430	8.2	83.1	12.9	60.0	v–NH

Table 4 Experimental and calculated vibrational Frequencies of PII in vacuum.

Mode	Frequency Exp.	unscaled	Scaled M1	scaled M2	FC	Relative IR intensity Exp.	Calc.	Raman activity	Assignment
1	–	54	53	109	0.0	–	0.0	0.3	Rot CH_3
2	–	62	61	117	0.0	–	0.3	0.3	Rot CH_3, Rot C≡N
3	–	82	81	135	0.0	–	1.1	0.2	Rot CH_3
4	–	126	124	175	0.1	–	2.1	3.0	δ–C≡N
5	–	173	170	218	0.1	–	1.4	0.5	ɣCH_3, ɣCN
6	–	203	199	245	0.1	–	0.1	0.8	τ–ring
7	–	228	224	269	0.1	–	3.7	0.4	τ–ring
8	–	277	272	313	0.1	–	0.4	0.3	δ–C–C
9	–	302	296	336	0.2	–	1.7	1.4	δ–C–C, δ–C–N
10	265	404	396	429	0.1	95.4	5.7	1.8	τ–NH2
11	–	432	423	455	0.7	–	0.2	6.8	ɣ–C–C, p–NH_2
12	–	452	443	473	0.5	–	0.8	1.4	δ–C≡N
13	–	464	454	484	0.4	–	4.2	3.1	ɣ–C–C, τ–NH_2
14	–	495	485	513	0.8	–	1.0	1.3	τ–ring
15	–	529	519	544	0.8	–	0.7	10.4	τ–ring
16	464	553	542	566	0.3	73.6	67.1	2.0	p–NH_2
17	547	574	562	585	0.7	88.9	26.5	0.6	τ–ring, p–NH_2
18	622	607	595	615	0.8	80.6	3.3	21.5	δ–C–C, δ–NH, δ– CH_3
19	–	622	609	628	1.2	–	0.5	6.8	δ–C–C, δ–NH, δ– CH_3
20	715	666	653	669	1.1	85.7	43.8	4.1	ring breathing
21	773	716	702	715	1.6	84.2	0.8	7.1	ring breathing
22	825	818	801	808	0.5	85.7	5.7	0.8	ɣC–H
23	–	972	952	949	1.7	–	2.8	4.3	p–NH_2, R– CH_3
24	951	991	971	966	1.2	86.1	1.8	6.6	p– CH_3
25	–	1040	1020	1011	0.9	–	0.5	0.2	p– CH_3
26	–	1046	1025	1016	0.9	–	0.3	2.5	τ– CH_3, p–NH_2
27	1029	1059	1038	1029	1.0	89.1	0.0	0.0	τ– CH_3
28	–	1103	1081	1069	2.0	–	2.2	1.2	δ– CH_3
29	1101	1133	1110	1096	1.5	88.3	0.6	1.4	δ–NH, w–NH_2
30	1177	1205	1181	1162	2.5	89.7	0.2	31.1	δ–CH, w–NH_2
31	–	1246	1221	1199	1.4	–	0.9	10.8	δ–CH
32	1374	1370	1343	1313	7.7	95.4	8.7	16.2	v–CC, v–C–N
33	–	1387	1359	1328	2.8	–	8.4	22.9	ɣ CH_3, ɣNH_2
34	–	1421	1393	1359	1.5	–	3.3	6.2	ɣ CH_3
35	–	1430	1401	1368	2.0	–	3.2	29.8	ɣ CH_3
36	–	1454	1425	1390	4.7	–	26.7	17.1	p– CH_3, v–C–N
37	1460	1488	1458	1421	1.4	97.0	2.6	8.6	τ CH_3,
38	–	1494	1464	1426	1.4	–	4.9	8.9	τ CH_3
39	–	1498	1468	1429	2.2	–	5.0	12.6	δ– CH_3
40	–	1513	1482	1443	1.7	–	47.3	14.9	δ– CH_3
41	1586	1517	1486	1447	2.2	100.0	3.5	6.0	δ– CH_3
42	–	1619	1587	1540	4.1	99.1	6.5	10.9	v–C=N, δ–NH_2, v–C=C
43	1586	1654	1621	1573	6.2	97.6	64.0	58.4	v–C=N, δ–NH_2,v–C=C
44	1657	1659	1626	1577	3.6	–	100.0	19.0	δ–NH_2
45	2211	2181	2051	2055	35.4	93.8	3.9	400.2	v–C≡N
46	–	3070	2886	2867	5.8	–	4.4	178.9	v– CH_3 (s.)
47	2749	3076	2891	2872	5.8	–	7.0	263.0	v– CH_3 (s.)
48	–	3147	2958	2938	6.4	–	2.2	56.1	v– CH_3 (as.)
49	–	3159	2970	2949	6.5	94.3	2.9	84.6	v–CH_3 (as.)
50	–	3175	2984	2963	6.5	98.2	4.5	48.6	v–CH_3 (as.)
51	2839	3176	2986	2964	6.6	98.7	4.8	60.0	v–CH_3 (as.)
52	3153	3220	3026	3004	6.7	97.6	2.4	100.2	v–CH (aromatic)
53	3329	3591	3375	3343	8.0	99.2	23.3	185.6	v–NH_2(s.)
54	3391	3715	3492	3457	9.0	99.1	17.9	36.4	v–NH_2 (as.)

The IR intensities were normalized to the strongest bands observed at 1586 cm^{-1}

Generally, scaling the calculated frequencies using the M2 method gives better agreement among the experimental and the scaled frequencies, therefore, hereafter unless differently specified we will discuss the calculated frequencies scaled by this method in comparison with the experimental ones. The presence of v–C–H stretching vibration is one of the distinctive mode for most of the heterocyclic aromatic compounds[68]. Two types of v–C–H modes are assigned in the compound PI corresponding to the aliphatic and the aromatic hydrogens. The asymmetrical aliphatic C–H modes appears at 3003 cm^{-l} in excellent agreement with the calculated value 3010 cm^{-1} while the symmetric mode is overestimated in calculation by ca. 85 cm^{-1}. On the other hand, the aromatic modes show a considerable agreement for the experimental and calculated values (3138 vs. 3098). The calculated values of v–C–H modes in compound PII deviate from their experimental values by ca. 100 cm^{-1}. This could be attributed to extend resonance structure of PII as depicted in Fig. 2. All the v–C–H modes in both molecules display high Raman activity due to the strong polarization. The in–plane C– δ–C–H bending vibration usually appears within 1300–1000 cm^{-1} while the out of plane mode (ɣ–C–H) [69] falls within 1000–750 cm^{-1}. On most cases these vibrations are coupled with others. For the PI molecule the δ–C–H and ɣ–C–H modes are observed at 1221 and 840 cm^{-1}, in good agreement with their calculated values 1205 and 798 cm^{-1}, respectively. Such agreement is also shown for PII where the calculated values for the δ–C–H and ɣ–C–H modes at 1162 and 808 cm^{-1} are nicely matching the experimental wavenumbers at 1177 and 825 cm^{-1}.

The exchange of OH and NH_2 in PI and PII, respectively, insignificantly affect the bond length of the nitrile group C≡N (1.18Å). Consequently, the starching mode of this group v–C≡N, characteristic by strong Raman activity, is observed nearly at the same frequency in both PI and PII (2217 and 2211 cm^{-1}) in matching with previously reported values[69-71]. The v–C–N modes show good agreement for the calculated and observed frequencies. Moreover, this mode is observed at slightly higher in energy (1425 cm^{-1}) in PI than the corresponding one in PII (1374 cm^{-1}), this difference could be attributed to more double bond character associated for the C–N bond in PI.

The theoretically calculated wave numbers of v–C=C modes in PI at 1569 and 1631 cm^{-1} concur well the experimentally observed values at 1536 and 1625 cm^{-1}. The same concurrent is also true in case of PII where the v–C=C mode is assigned at 1586 and 1573 cm^{-1} for the experiential and calculated values, respectively. The ring breathing is a characteristic mode for cyclic aromatic molecules, this band is usually strong and appear in the range 700–750 cm^{-1}. Such band with strong intensity appears in both PI and PII in the range 715–773 cm^{-1}. The scaled wave numbers calculated for this mode being 702 and 669/715 for PI and PII, respectively, in a goodagreement with the observed values.

The strong band observed at 3434 cm^{-1} for the v–N–H mode of PI perfectly matches the calculated value at 3430 cm^{-1}. In PII instead, two v–N–H modes appear experimentally at 3329 and 3391 cm^{-1} due to the symmetric and asymmetric vibration of the NH_2 group, these bands coincide with the theoretical ones calculated at 3343 and 3457 cm^{-1}, respectively. The strong bands due to δ–NH_2 bending modes in PII are calculated at 1540, 1573 and 1577 cm^{-1} in coupling with the v–C=C and v–C=N showing considerable agreement with the experimental results. On the other hand, the strongest IR band in PI is assigned to the v–C=O, the calculated value deviates by ca. 58 cm^{-1} from the experimental value 1659. This deviation is attributed to the coupling of this mode with the in–plane binding of δ–C–H mode.

Experimental Data

3–cyano–4,6–dimethyl–2–pyridone (PI)

White crystals, mp: 293–295°C; IR (KBr) cm^{-1}: 3434 (NH), 3138 (C–H aromatic), 3003 (C–H aliphatic), 2217 (–C≡N), 1659 (C=O), 1625 (C=C); ^1H NMR (DMSO–d_6) δ ppm: 2.18 (s, 3H,–CH_3), 2.26 (s, 3H,–CH_3), 6.12 (s, 1H, pyridine–H), 12.28 (s, 1H, NH (D_2O exchangeable)); MS: *m/z* 148 (M^+,100%); Anal. Calcd for $C_8H_8N_2O$ (148): C, 64.86; H, 5.41; N, 18.92. Found: C, 65.01; H, 5.32; N, 18.71.

2–Amino–3–cyano–4,6–dimethylpyridine (PII)

Yellow crystals, mp: 256–258°C; IR (KBr) cm^{-1}: 3391, 3330 (NH_2), 3153 (C–H aromatic), 2839, 2749 (C–H aliphatic), 2213 (–C≡N), 1656 (NH bending),1589, 1568 (C=C, C=N); ^1H NMR (DMSO–d_6) δ ppm: 2.22 (s, 3H,–CH_3), 2.24 (s, 3H,–CH_3), 6.4 (s, 1H, pyridine–H), 6.63 (s, 2H, NH_2 (D_2O exchangeable)); ^{13}C NMR (DMSO–d_6) δ ppm: 19.74

(aliphatic CH_3 at 4), 24.14 (aliphatic CH_3 at 6), 87.01 (pyridine C bearing CN), 112.94 (–C≡N), 116.55, 152.40, 160.09, 161.49 (pyridine carbons); Anal. Calcd for $C_8H_9N_3$ (147): C, 65.31; H, 6.12; N, 28.57. Found: C, 65.08; H, 6.20; N, 28.61.

Conclusion

In conclusion, a facile, simple and efficient one–pot protocol for the synthesis of 3–cyano–4,6–dimethyl–2–pyridone (PI) and 2–amino–3–cyano–4,6–dimethylpyridine (PII) using acetyl acetone, malononitrile and ammonium acetate is reported. Ammonium acetate acts as a base in PI synthesis and nitrogen source in PII synthesis. This method offers several advantages as shorter reaction time, high yields and easy work up. The effect of solvent, ammonium acetate concentration and reaction time on the products yield were studied. The synthesized compounds as well as reactants and intermediates were investigated at the MP2/6–311++G(d,p) level of theory. Calculations provide a clear explanation for the reaction mechanism in gas phase, ethanol and acetic acid. No significant effects for the geometrical parameter, charges or spectroscopic properties were encountered due the solvent effects. Two different methods have been applied to scale the computed vibrational frequencies of the investigated compound. The calculated scaled frequencies are in good agreement with the experimental results with a correlation coefficient R^2=0.99 for both PI and PII, supporting the reliability of the method used in the calculations.

References

[1] A. Srivastava, S. Pandeya, Indole" a versatile nucleuse in pharmaceutical field, Int. J. Curr. Pharm. Rev. Res 4 (2011) 5-8.
[2] N.B. Patel, S.N. Agravat, F.M. Shaikh, Synthesis and antimicrobial activity of new pyridine derivatives-I, Med. Chem. Res. 20(7) (2011) 1033-1041.
[3] N.B. Patel, S.N. Agravat, Synthesis and Antimicrobial Studies of New Pyridine Derivatives, Chem. Heterocycl. Comp. 45(11) (2009) 1343-1353.
[4] A.M.R. Bernardino, A.R. de Azevedo, L.C.D. Pinheiro, J.C. Borges, V.L. Carvalho, M.D. Miranda, M.D.F. de Meneses, M. Nascimento, D. Ferreira, M.A. Rebello, V.A.G.G. da Silva, I.C.P.P. de Frugulhetti, Synthesis and antiviral activity of new 4-(phenylamino)/4-[(methylpyridin-2-yl)amino]-1-phenyl-1H-pyrazolo[3,4-b]pyridine-4-carboxylic acids derivatives, Med. Chem. Res. 16(7-9) (2007) 352-369.
[5] E. Paronikyan, A. Noravyan, I. Dzhagatspanyan, I. Nazaryan, R. Paronikyan, Synthesis and anticonvulsant activity of isothiazolo [5, 4-b] pyrano (thiopyrano)[4, 3-d] pyridine and isothiazolo [4, 5-b]-2, 7-naphthyridine derivatives, Pharm. Chem. J. 36(9) (2002) 465-467.
[6] T.J. Tucker, J.T. Sisko, R.M. Tynebor, T.M. Williams, P.J. Felock, J.A. Flynn, M.-T. Lai, Y. Liang, G. McGaughey, M. Liu, Discovery of 3-{5-[(6-amino-1 H-pyrazolo [3, 4-b] pyridine-3-yl) methoxy]-2-chlorophenoxy}-5-chlorobenzonitrile (MK-4965): a potent, orally bioavailable

HIV-1 non-nucleoside reverse transcriptase inhibitor with improved potency against key mutant viruses, J. Med. Chem. 51(20) (2008) 6503-6511.
[7] F. Zhang, Y.F. Zhao, L. Sun, L. Ding, Y.C. Gu, P. Gong, Synthesis and anti-tumor activity of 2-amino-3-cyano-6-(1H-indol-3-yl)-4-phenylpyridine derivatives in vitro, Eur. J. Med. 46(7) (2011) 3149-3157.
[8] T. Murata, M. Shimada, S. Sakakibara, T. Yoshino, H. Kadono, T. Masuda, M. Shimazaki, T. Shintani, K. Fuchikami, K. Sakai, H. Inbe, K. Takeshita, T. Niki, M. Umeda, K.B. Bacon, K.B. Ziegelbauer, T.B. Lowinger, Discovery of novel and selective IKK-beta serine-threonine protein kinase inhibitors. Part 1, Bioorg. Med. Chem. Lett. 13(5) (2003) 913-8.
[9] H. Sheibani, K. Saidi, M. Abbasnejad, A. Derakhshani, I. Mohammadzadeh, A convenient one-pot synthesis and anxietic activity of 3-cyano-2(1H)-iminopyridines and halogen derivatives of benzo[h] chromenes, Arab. J. Chem. 9 (2016) S901-S906.
[10] D. Vyas, S. Tala, J. Akbari, M. Dhaduk, K. Joshi, H. Joshi, Synthesis and antimicrobial activity of new cyanopyridine and cyanopyrans towards Mycobacterium tuberculosis and other microorganisms, Indian. J. Chem., Sec. B 48 (2009) 833-839.
[11] T. Murata, M. Shimada, H. Kadono, S. Sakakibara, T. Yoshino, T. Masuda, M. Shimazaki, T. Shintani, K. Fuchikami, K.B. Bacon, Synthesis and structure–activity relationships of novel IKK-β inhibitors. Part 2: improvement of in vitro activity, Bioorg. Med. Chem. Lett. 14(15) (2004) 4013-4017.
[12] M. Ravinder, B. Mahendar, S. Mattapally, K.V. Hamsini, T.N. Reddy, C. Rohit, K. Srinivas, S.K. Banerjee, V.J.J.B. Rao, m.c. letters, Synthesis and evaluation of novel 2-pyridone derivatives as inhibitors of phosphodiesterase3 (PDE3): A target for heart failure and platelet aggregation, 22(18) (2012) 6010-6015.
[13] Z. Lv, Y. Zhang, M. Zhang, H. Chen, Z. Sun, D. Geng, C. Niu, K.J.E.j.o.m.c. Li, Design and synthesis of novel 2'-hydroxy group substituted 2-pyridone derivatives as anticancer agents, 67 (2013) 447-453.
[14] S.K. Rai, S. Khanam, R.S. Khanna, A.K.J.C.G. Tewari, Design, Design and Synthesis of 2-Pyridone Based Flexible Dimers and Their Conformational Study through X-ray Diffraction and Density Functional Theory: Perspective of Cyclooxygenase-2 Inhibition, 15(3) (2015) 1430-1439.
[15] V. Aberg, P. Das, E. Chorell, M. Hedenstrom, J.S. Pinkner, S.J. Hultgren, F. Almqvist, Carboxylic acid isosteres improve the activity of ring-fused 2-pyridones that inhibit pilus biogenesis in E-coli, Bioorg. Med. Chem. Lett. 18(12) (2008) 3536-3540.
[16] J.S. Pinkner, H. Remaut, F. Buelens, E. Miller, V. Aberg, N. Pemberton, M. Hedenstrom, A. Larsson, P. Seed, G. Waksman, S.J. Hultgren, F. Almqvist, Rationally designed small compounds inhibit pilus biogenesis in uropathogenic bacteria, Proc. Natl. Acad. Sci. U. S. A. 103(47) (2006) 17897-902.
[17] V. Åberg, M. Sellstedt, M. Hedenström, J.S. Pinkner, S.J. Hultgren, F. Almqvist, Design, synthesis and evaluation of peptidomimetics based on substituted bicyclic 2-pyridones—Targeting virulence of uropathogenic E. coli, Biorg. Med. Chem. 14(22) (2006) 7563-7581.
[18] V. Aberg, M. Hedenstrom, J.S. Pinkner, S.J. Hultgren, F. Almqvist, C-Terminal properties are important for ring-fused 2-pyridones that interfere with the chaperone function in uropathogenic E-coli, Org. Biomol. Chem. 3(21) (2005) 3886-3892.
[19] Y. Fujita, H. Oguri, H. Oikawa, Biosynthetic studies on the antibiotics PF1140: a novel pathway for a 2-pyridone framework, Tetrahedron Lett. 46(35) (2005) 5885-5888.
[20] E. Verissimo, N. Berry, P. Gibbons, M.L. Cristiano, P.J. Rosenthal, J. Gut, S.A. Ward, P.M. O'Neill, Design and synthesis of novel 2-pyridone peptidomimetic falcipain 2/3 inhibitors, Bioorg. Med. Chem. Lett. 18(14) (2008) 4210-4.
[21] K. Barral, J. Balzarini, J. Neyts, E. De Clercq, R.C. Hider, M. Camplo, Synthesis and antiviral evaluation of cyclic and acyclic 2-methyl-3-hydroxy-4-pyridinone nucleoside derivatives, J. Med. Chem. 49(1) (2006) 43-50.
[22] A.Z.A. Elassar, Synthesis and reactions of 3-cyano-4, 6-dimethyl-2-pyridone, J. Heterocycl. Chem. 48(2) (2011) 272-278.

[23] V.B. Rybakov, A.A. Bush, E.V. Babaev, L.A. Aslanov, 3-Cyano-4,6-dimethyl-2-pyridone (Guareschi pyridone), Acta Crystallogr. E. 60(2) (2004) O160-O161.
[24] E. Semichenko, F. Vasilenko, M. Tovbis, E.Y.J.R.J.o.O.C. Belyae, Zeolites in the Synthesis of 1-Alkyl-2-oxonicotinonitriles, 41(2) (2005) 313-314.
[25] A.Z.A. Elassar, Synthesis and reactions of 3-cyano-4, 6-dimethyl-2-pyridone, J Journal of Heterocyclic Chemistry 48(2) (2011) 272-278.
[26] F. Yassin, Synthesis, reactions and biological activity of 2-substituted 3-cyano-4, 6-dimethylpyridine derivatives, J Chemistry of heterocyclic compounds 45(1) (2009) 35-41.
[27] M.W. Beukers, I. Meurs, A.P. Ijzerman, Structure-affinity relationships of adenosine A2B receptor ligands, Med. Res. Rev. 26(5) (2006) 667-98.
[28] E.V. Verbitskiy, E.M. Cheprakova, M.G. Pervova, G.G. Danagulyan, G.L. Rusinov, O.N. Chupakhin, V.N. Charushin, Synthesis of 6-thienyl-substituted 2-amino-3-cyanopyridines, Russ. Chem. Bull. 64(3) (2015) 689-694.
[29] M. Mantri, O. de Graaf, J. van Veldhoven, A. Göblyös, J.K. von Frijtag Drabbe Künzel, T. Mulder-Krieger, R. Link, H. de Vries, M.W. Beukers, J. Brussee, 2-Amino-6-furan-2-yl-4-substituted nicotinonitriles as A2A adenosine receptor antagonists, J. Med. Chem. 51(15) (2008) 4449-4455.
[30] D. Anderson, N. Stehle, S. Kolodziej, E. Reinhard, I. PCT, Appl. 2004, WO 2004055015 A1 20040701, Chem. Abstr, 2004, p. 89018.
[31] P.T. Patil, P.P. Warekar, K.T. Patil, S.S. Undare, D.K. Jamale, S.S. Vibhute, N.J. Valekar, G.B. Kolekar, M.B. Deshmukh, P.V.J.R.o.C.I. Anbhule, A simple and efficient one-pot novel synthesis of pyrazolo[3,4-b][1,8]naphthyridine and pyrazolo[3,4-d]pyrimido[1,2-a]pyrimidine derivatives as anti-inflammatory agents, Res. Chem. Intermed. 44(2) (2018) 1119-1130.
[32] K. Ghoneim, M. Badran, M. Shaaban, S. El-Meligie, Novel thienyl substituted pyridone and pyridine derivatives, synthesis and antimicrobial activity, Egypt J Pharm Sci 29 (1988) 553-561.
[33] M.M. Ghorab, A.Y. Hassan, Synthesis and antibacterial properties of new dithienyl containing pyran, pyrano[2,3-b] pyridine, pyrano[2,3-d]pyrimidine and pyridine derivatives, Phosphorus Sulfur 141(1) (1998) 251-261.
[34] P. Verma, N. Kumar, S. Bhargava, A.K. Yadav, Synthesis and antimicrobial screening of some new pyrido [2,3-d] pyrimidines and their ribofuranosides, Indian J. Heterocycl. Chem. 16(4) (2007) 387-390.
[35] D. Mungra, M. Patel, R. Patel, Arkivoc 2009,(xiv), 64.
[36] S.K. Elsaedany, M. AbdEllatif Zein, E.M. AbedelRehim, R.M. Keshk, Synthesis, Anti-Microbial, and Cytotoxic Activities Evaluation of Some New Pyrido [2, 3-d] Pyrimidines, J. Heterocycl. Chem. 53(5) (2016) 1534-1543.
[37] R. Ramesh, P. Vadivel, S. Maheswari, A.J.R.o.C.I. Lalitha, Click and facile access of substituted tetrahydro-4H-chromenes using 2-aminopyridine as a catalyst, 42(10) (2016) 7625-7636.
[38] X. Meng, Y. Wang, C. Yu, P.J.R.A. Zhao, Heterogeneously copper-catalyzed oxidative synthesis of imidazo [1, 2-a] pyridines using 2-aminopyridines and ketones under ligand-and additive-free conditions, REC Adv. 4(52) (2014) 27301-27307.
[39] M. Jeeva, M.S. Boobalan, G.V. Prabhu, Adsorption and anticorrosion behavior of 1-((pyridin-2-ylamino)(pyridin-4-yl)methyl)pyrrolidine-2,5-dione on mild steel surface in hydrochloric acid solution, Res. Chem. Intermed. 44(1) (2018) 425-454.
[40] F. Shi, S.J. Tu, F. Fang, T.J. Li, One-pot synthesis of 2-amino-3-cyanopyridine derivatives under microwave irradiation without solvent, ARKIVOC 1 (2005) 137-142.
[41] S.J. Tu, H. Jiang, Q.Y. Zhuang, C.B. Miao, D.Q. Shi, X.S. Wang, Y. Gao, One-pot synthesis of 2-amino-3-cyano-4-aryl-7,7-dimethyl-5-oxo-5,6,7,8-tetrahydro-4H-benzo[b]pyran under ultrasonic irradiation without catalyst, Chinese J. Org. Chem. 23(5) (2003) 488-490.
[42] W.J. Zhou, S.J. Ji, Z.L. Shen, An efficient synthesis of ferrocenyl substituted 3-cyanopyridine derivatives under ultrasound irradiation, J. Organomet. Chem. 691(7) (2006) 1356-1360.

[43] T.S. Jin, A.Q. Wang, F. Shi, L.S. Han, L.B. Liu, T.S. Li, Hexadecyldimethyl benzyl ammonium bromide: an efficient catalystfor a clean one-pot synthesis of tetrahydrobenzopyran derivatives in water, ARKIVOC 14 (2006) 78-86.
[44] A.M. Shestopalov, O.A. Naumov, Synthesis of substituted 2-amino-3-cyano-7,9-dimethyl-4H-pyrano[2 ',3 ': 4,5]thieno[2,3-b]pyridines, Russ. Chem. Bull. 52(6) (2003) 1380-1385.
[45] C. Møller, M.S. Plesset, Note on an approximation treatment for many-electron systems, Phys. Rev. 46(7) (1934) 618.
[46] M. Awad, M. Masoud, M. Shaker, A.E. Ali, M.J.R.o.C.I. El-Tahawy, MP2 and DFT theoretical studies of the geometry, vibrational and electronic absorption spectra of 2-aminopyrimidine, 39(6) (2013) 2741-2761.
[47] A. Müller, M. Losada, S. Leutwyler, Ab Initio Benchmark Study of (2-Pyridone)2, a Strongly Bound Doubly Hydrogen-Bonded Dimer, The Journal of Physical Chemistry A 108(1) (2004) 157-165.
[48] N.A.J.A.J.o.C. Wazzan, DFT and MP2 Study of Geometry, IR and UV-Visible Spectroscopy and First Hyperpolarizability of 2-Aminopyridine, 3-Aminopyridine and 4-Aminopyridine in Gas Phase and in Solvents, 27(12) (2015) 0000-0000.
[49] A.D. McLean, G.S. Chandler, Contracted Gaussian basis sets for molecular calculations. I. Second row atoms, Z=11–18, J. Chem. Phys. 72(10) (1980) 5639-5648.
[50] R. Krishnan, J.S. Binkley, R. Seeger, J.A. Pople, Self-consistent molecular orbital methods. XX. A basis set for correlated wave functions, J. Chem. Phys. 72(1) (1980) 650-654.
[51] E. Cances, B. Mennucci, J. Tomasi, A new integral equation formalism for the polarizable continuum model: Theoretical background and applications to isotropic and anisotropic dielectrics, J. Chem. Phys. 107(8) (1997) 3032-3041.
[52] D. Chatfield, Christopher J. Cramer: Essentials of Computational Chemistry: Theories and Models, Theoretical Chemistry Accounts: Theory, Computation, and Modeling (Theoretica Chimica Acta) 108(6) (2002) 367-368.
[53] Y. Lı, Modeling solvent effects on excitation energies for polyenes, Bilkent University, 2006.
[54] G.W.T. M. J. Frisch, H. B. Schlegel, G. E. Scuseria, M. A. Robb, J. R. Cheeseman, G. Scalmani, V. Barone, B. Mennucci, G. A. Petersson, H. Nakatsuji, M. Caricato, X. Li, H. P. Hratchian, A. F. Izmaylov, J. Bloino, G. Zheng, J. L. Sonnenberg, M. Hada, M. Ehara, K. Toyota, R. Fukuda, J. Hasegawa, M. Ishida, T. Nakajima, Y. Honda, O. Kitao, H. Nakai, T. Vreven, J. A. Montgomery, Jr., J. E. Peralta, F. Ogliaro, M. Bearpark, J. J. Heyd, E. Brothers, K. N. Kudin, V. N. Staroverov, R. Kobayashi, J. Normand, K. Raghavachari, A. Rendell, J. C. Burant, S. S. Iyengar, J. Tomasi, M. Cossi, N. Rega, J. M. Millam, M. Klene, J. E. Knox, J. B. Cross, V. Bakken, C. Adamo, J. Jaramillo, R. Gomperts, R. E. Stratmann, O. Yazyev, A. J. Austin, R. Cammi, C. Pomelli, J. W. Ochterski, R. L. Martin, K. Morokuma, V. G. Zakrzewski, G. A. Voth, P. Salvador, J. J. Dannenberg, S. Dapprich, A. D. Daniels, Ö. Farkas, J. B. Foresman, J. V. Ortiz, J. Cioslowski, and D. J. Fox, (Gaussian 09 (Gaussian, Inc., Wallingford CT, 2009).).
[55] P. Beak, Energies and alkylations of tautomeric heterocyclic compounds: old problems-new answers, Acc. Chem. Res. 10(5) (1977) 186-192.
[56] M.J. Field, I.H. Hillier, Non-dissociative proton transfer in 2-pyridone–2-hydroxypyridine. An ab initio molecular orbital study, Journal of the Chemical Society, Perkin Transactions 2 (5) (1987) 617-622.
[57] A. Held, B. Champagne, D. Pratt, Inertial axis reorientation in the S 1← S 0 electronic transition of 2-pyridone. A rotational Duschinsky effect. Structural and dynamical consequences, J. Chem. Phys. 95(12) (1991) 8732-8743.
[58] A. Held, D.W. Pratt, The 2-Pyridone Dimer, a Model Cis Peptide - Gas-Phase Structure from High-Resolution Laser Spectroscopy, J. Am. Chem. Soc. 112(23) (1990) 8629-8630.
[59] H.W. Yang, B.M. Craven, Charge density study of 2-pyridone, Acta Crystallogr. B 54 (Pt 6)(6) (1998) 912-20.

[60] O. Kennard, D. Watson, F. Allen, N. Isaacs, W.D.S. Motherwell, R. Pettersen, W. Town, Molecular Structures and Dimensions (International Union of Crystallography), Vol, A1 (NVA Oosthoek's Uitgevers Mij. Utrecht) (1972).
[61] M. Chao, E. Schemp, R.D. Rosenstein, 2-Aminopyridine, Acta Crystall.L B-Stru. 31(12) (1975) 2922-2924.
[62] D. Mootz, H.G. Wussow, Crystal structures of pyridine and pyridine trihydrate, J. Chem. Phys. 75(3) (1981) 1517-1522.
[63] M. Masoud, M. Awad, A.E. Ali, M.J.J.o.M.S. El-Tahawy, Molecular structure of amino alcohols on aluminum surface, 1063 (2014) 51-59.
[64] K. Fukui, T. Yonezawa, H. Shingu, A Molecular Orbital Theory of Reactivity in Aromatic Hydrocarbons, 20(4) (1952) 722-725.
[65] K. Balci, S. Akyuz, A theoretical vibrational spectroscopic study with density functional theory and force field refinement calculation methods on free 4-aminopyrimidine molecule, J. Mol. Struct. 744 (2005) 909-919.
[66] M.D. Halls, J. Velkovski, H.B. Schlegel, Harmonic frequency scaling factors for Hartree-Fock, S-VWN, B-LYP, B3-LYP, B3-PW91 and MP2 with the Sadlej pVTZ electric property basis set, Theor. Chem. Acc. 105(6) (2001) 413-421.
[67] M.K. Awad, M.S. Masoud, M.A. Shaker, A.E. Ali, M.M.T. El-Tahawy, MP2 and DFT theoretical studies of the geometry, vibrational and electronic absorption spectra of 2-aminopyrimidine, Res. Chem. Intermed. 39(6) (2013) 2741-2761.
[68] G. Varsányi, M.A.e. Kovner, L. Láng, Assignments for vibrational spectra of 700 benzene derivatives, Akademiai Kiado1973.
[69] M. Kurt, P.C. Babu, N. Sundaraganesan, M. Cinar, M.J.S.A.P.A.M. Karabacak, B. Spectroscopy, Molecular structure, vibrational, UV and NBO analysis of 4-chloro-7-nitrobenzofurazan by DFT calculations, 79(5) (2011) 1162-1170.
[70] A.R. Krishnan, H. Saleem, S. Subashchandrabose, N. Sundaraganesan, S.J.S.A.P.A.M. Sebastain, B. Spectroscopy, Molecular structure, vibrational spectroscopic (FT-IR, FT-Raman), UV and NBO analysis of 2-chlorobenzonitrile by density functional method, 78(2) (2011) 582-589.
[71] S. Sudha, N. Sundaraganesan, M. Kurt, M. Cinar, M.J.J.o.M.S. Karabacak, FT-IR and FT-Raman spectra, vibrational assignments, NBO analysis and DFT calculations of 2-amino-4-chlorobenzonitrile, 985(2-3) (2011) 148-156.